Influence of the electrolytic medium on the performance and stability of functionalized graphene-polypyrrole nanocomposites as materials for supercapacitors

Yahdi Bin Rus, Laurent Galmiche, Pierre Audebert, Fabien Miomandre

Influence of the electrolytic medium on the performance and stability of functionalized graphene-polypyrrole nanocomposites as materials for supercapacitors

Yahdi Bin Rus, Laurent Galmiche, Pierre Audebert, Fabien Miomandre*

PPSM, CNRS – ENS Paris-Saclay, 61 Avenue Président Wilson 94235 Cachan (France)

mioman@ens-paris-saclay.fr

Abstract

Nanocomposites made of functionalized graphene with polypyrrole were synthesized in two steps by first incorporating pyridine-pyridazine functions on graphene surface through cycloaddition followed by electropolymerization of pyrrole in acetonitrile. The specific capacitance of the material was measured by galvanic charge-discharge cycles and the stability upon cycling investigated in various electrolytic media (acetonitrile, ionic liquid, acidic and neutral water) in comparison with non-functionalized graphene with or without polypyrrole. While acetonitrile reveals pure capacitive behavior for all materials investigated, acidic water is the medium where the capacitance values are the highest and surprisingly where nanocomposites with polypyrrole show a better capacitance retention upon cycling than graphene alone. A positive impact of graphene functionalization prior to electropolymerization was demonstrated in all electrolytic media (capacitance losses limited to less than 8% after 1500 cycles in all media but neutral water), highlighting the interest of interface control in this kind of nanocomposites.

Introduction

Conducting polymers have been used for energy storage for more than 3 decades now, firstly as materials for batteries due to their ability to be electrochemically doped and dedoped reversibly. However, due to their limited energy storage per mass (only 25 to 30% doping per repeating unit in most cases), they appeared more promising for supercapacitors[1], taking benefit of their mixed faradaic and capacitive behavior. Indeed, supercapacitors, as intermediate systems between high energy (batteries) and high power (capacitors) devices, are usually classified into electrical double layer (EDL) based capacitors on one hand and pseudo-capacitors involving faradaic reactions on the other hand[2]. While EDL systems are very stable as they do not involve any chemical changes in the active material, capacitance values are usually limited and in that framework adding a faradaic component highly improves the performance, unfortunately usually to the detriment of the long term stability. Therefore, a reasonable trade-off would be to mix carbonaceous nanomaterials with conducting polymers in nanocomposites to take benefit of the advantages of both materials and even hope possible synergetic effects[3, 4]. This topic was recently reviewed in the framework of supercapacitors[5]. Among the various conducting polymers available, polypyrrole (PPy) has a certain number of advantages like its low cost, its possibility to be electrochemically synthesized in various polar media including water, and a reasonably good stability of its properties under ambient atmosphere[6, 7]. Thus, numerous nanocomposites combining carbon nanotubes[8-10] or more recently graphene oxide[11], reduced graphene oxide[12, 13] or even both of them[14] with PPy have been designed and their capacitance measured either in 3- electrode or in coin cells.

Our own approach consists in functionalizing highly reduced graphene oxide in order to improve the compatibility with PPy and create interlayer spacing for the insertion of PPy. Our starting material is called FGS20 (Functional Graphene Sheet with C/O equal to 20): it is a highly reduced graphene oxide obtained by the Hummer's method followed by thermal treatment[15, 16] which behaves at the end as a two-dimensional polyene with very few functional groups. We previously demonstrated that

introducing chemical functions like pyridine-pyridazine through cycloaddition reactions from a tetrazine core compound led to nanocomposites with PPy showing good thermal and electrochemical properties and high capacitance values[17]. However, the weak point remained the long term stability. Therefore, we were interested in investigating the role of the electrolytic medium on this aspect, an important point which has been the topic of very few systematic studies in the literature so far[18-19].

We have chosen to compare an organic solvent (acetonitrile) with neutral or acidic water and a mixture of acetonitrile and ionic liquid ($BMIMPF_6$) as possible electrolytic media for cycling. Moreover, the role of the graphene functionalization itself was also considered as we systematically compared the results of nanocomposites with those using a simple mixture of PPy with reduced graphene.

Experimental section

Graphene functionalization

FGS20-bpp is synthesized as follows [17]: Firstly, FGS20 is dispersed in dichloroethane (10 mL) by ultrasonication (specific horn, power 35-40%) for 30 minutes in ice bath to keep the temperature low. Separately, bis-2-pyridine-1,2,4,5-tetrazine (bptz) (11 mg) is dissolved in acetonitrile solution (6 mL) and then mixed with the as-prepared FGS20 dispersion in a 30 mL microwave reaction vessel. The microwave-assisted reaction takes place at 120°C under 600 rpm stirring for 1 hour. In the first few minutes of reaction, the temperature is controlled to raise step by step from 60°C to 120°C (20 °C/3 min), and then kept at 120°C for the remaining 51 minutes. After cooling down, the obtained FGS20-bpp dispersion is washed with dichloromethane until the supernatant becomes colorless. Finally, the product is dried under vacuum.

FGS20-PPy electrosynthesis

First, FGS20-bpp is dispersed in dichloromethane (ca. 1 mg/mL) for 3 to 5 minutes under sonication, then coated onto INOX plates and finally dried for several hours to ensure that FGS20-bpp is tightly attached to the INOX surface. Fresh pyrrole was then added to acetonitrile with tetrabutylammonium hexafluorophosphate $TBAPF_6$ (0.01 M) as the supporting electrolyte. Finally, electrochemical polymerization is performed by using CV between 0 V and at most 1.0 V to prevent overoxidation during electropolymerization, at 100 mV/s for 20 cycles. CV is conducted in a three-electrode electrochemical cell, using INOX as the working electrode (1 cm × 10 cm) with FGS20-bpp (1 cm × 1 cm) coated on it, an Ag wire as the pseudo-reference electrode and a large area (ca. 10 cm^2) platinum sheet as the counter electrode (see scheme 1). The number of cycles was optimized in a previous study[17] but as the working electrode is different the final features of the electrogenerated material might be slightly different. Therefore, TGA analysis was performed to estimate the amount of PPy in the final nanocomposite. FGS20/PPy is prepared exactly the same way, starting from the same dispersion (1 mg/mL) and applying the same number of electropolymerization cycles.

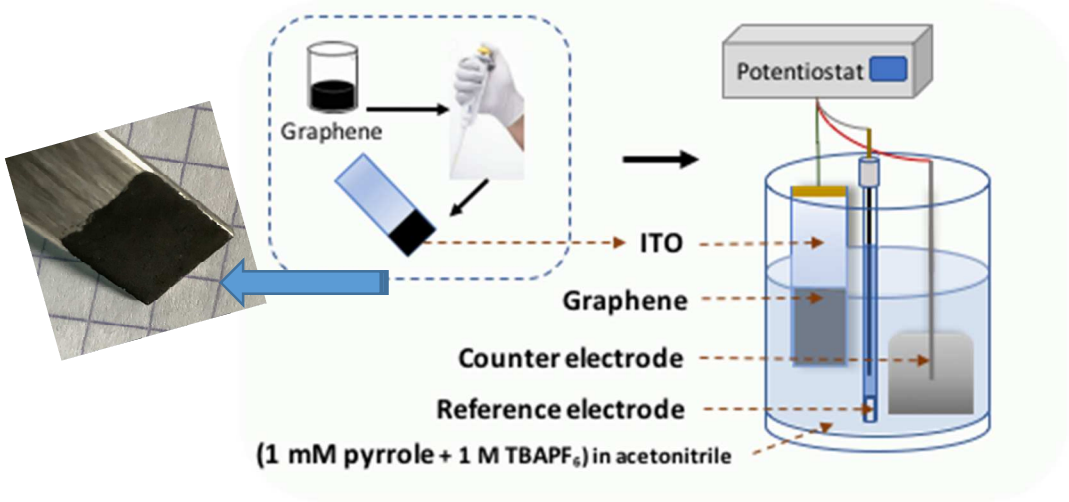

Scheme 1: Set-up used for electrosynthesis of FGS-PPy nanocomposites and snapshot of the coated INOX electrode.

Stability test

Capacitance values of all samples were measured from cyclic voltammetry (CV) and galvanostatic charge-discharge (GCD) tests in four different media: acetonitrile (ACN) with $TBAPF_6$ as the supporting electrolyte (0.1 M), sulfuric acidic (0.01 M) and sodium sulfate (0.1 M) aqueous electrolytes, and finally 1-butyl-3-methylimidazolium hexafluorophosphate ($BMIMPF_6$) ionic liquid mixed with 25% of ACN to reduce the viscosity. Stability tests were performed using CV during 1500 cycles (CHInstruments potentiostat) and following the capacitance retention upon cycling. Specific capacitance was also measured in three-electrode cells from GCD cycles by applying constant current in the range [1.0-1.3] $A.g^{-1}$ with an EG&G 273 (Princeton Applied Research) Potentiostat/Galvanostat. Both stability tests and capacitance measurements are performed with non-aqueous Ag^{+}/Ag or aqueous SCE reference electrodes depending on the electrolytic medium.

Thermogravimetric analysis (TGA)

Thermal stability of all samples was evaluated with a thermogravimetric analyzer (Pyris 6 TGA). FGS20-bpp/PPy on ITO surface was dried at 30°C under vacuum for 30 minutes before measurement. FGS20-bpp/PPy was then removed from ITO by carefully peeling the product manually and collected into the TGA furnace for thermal analysis. The amount of materials for analysis is around 1.2 mg for all samples. The mass change was then observed over time as the temperature changes from 30°C to 800°C at 20°C/min. The environment was kept inert by applying nitrogen flow (20 mL/min) during the measurement.

FTIR

FTIR spectra of all samples were measured by using Nicolet Nexus FT-IR. The samples are characterized directly on the material powder after peeling from the ITO surface.

Results and discussion

Synthesis and characterization of the materials

FGS-bpp is synthesized in one step from FGS20 and bis-2-pyridine-1,2,4,5-tetrazine (bptz) by an inverse demand Diels-Alder reaction, which has proven to be very efficient with this type of tetrazine derivative[20]. The reaction outcome is shown in scheme 2. After cycloaddition with nitrogen gas evolution, a bis-2-pyridine-pyridazine (bpp) moiety is grafted covalently through the pyridazine ring on the polyene structure of FGS20.

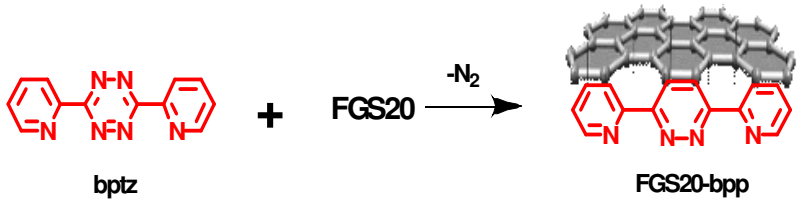

Scheme 2 : Inverse demand Diels-Alder reaction leading to FGS20-bpp where graphene is functionalized by bispyridinepyridazine.

Figure S1 shows the typical CVs recorded during the electrosynthesis of FGS20-PPy nanocomposites. PPy growth is clearly visible from the gradual increase of current in the 0.1-0.8 V range at each cycle. The electropolymerization is stopped after 20 cycles. The synthetic charge can be extracted by integrating the anodic current over all the cycles[21], giving a value of 16.9 mC cm^{-2}. Electropolymerized pyrrole weight m was calculated with the following equation

$$m = \frac{\mathrm{MQ}}{2.3\ \mathrm{F}}$$

where M is the molar mass of doped pyrrole plus the anion, Q is the coulombic charge per electrode area unit, F is the Faraday constant (96500 C mol^{-1}) and assuming the doping level of PPy to 30% so that the overall number of electrons exchanged is 2.3. Based on this equation, the weight m of polymer produced on the working electrode after 20 cycles of cyclic voltammetry in ACN+$TBAPF_6$ can be estimated to be equal to 16 µg, assuming an electropolymerization yield of 100%.

Figure 1 shows the FTIR spectra of the pristine graphene (FGS20), tetrazine precursor (bptz), functionalized graphene (FGS20-bpp) and the final nanocomposite (FGS20-bpp/PPy). FGS20 shows a featureless spectrum where only the aromatic C=C (1570 cm^{-1}) and C-C (1094 cm^{-1}) elongation vibrations can be seen. Bptz shows characteristic peaks ascribed to pyridine (744, 796 cm^{-1}) and tetrazine (1390 and 1130 cm^{-1}) subunits. The two latter bands are much weaker in the spectrum of FGS20-bpp showing that bptz has actually reacted through the tetrazine ring. A shift in the vibration band of aromatic C=C of the graphene subunit can be seen since the broad band is now centered at 1560 cm^{-1}. Moreover, the two peaks located at 1615 and 1742 cm^{-1} can be assigned to the phthalazine structure, created from cycloaddition between tetrazine as the diene and graphene as the dienophile in the inverse demand Diels-Alder reaction[20]. A shift in the broad band due to C-C vibration of graphene is also visible (from 1094 to 1066 cm^{-1}). The spectrum of FGS-bpp/PPy nanocomposite displays the main features of PPy: the two bands located at 1533 and 1456 cm^{-1} are consistent with antisymmetric and symmetric pyrrole ring vibrations[17], the one at 1295 cm^{-1} with C-N vibration and those at 1152 and 1011 cm^{-1} with C-C vibration bands.

Figure 2 shows the thermogravimetric properties of the various materials. Functionalizing graphene by bpp leads to a slight increase of the weight loss compared to FGS20 (6% vs. 3.8%), which is consistent with an increase of the more thermosensitive organic part in modified graphene. Besides it is clear that mixing PPy with non-functionalized FGS20 leads to a sharp weight loss (15%) starting at 200°C up to 340°C which can be ascribed to the polymer in the composite. Functionalized graphene-PPy composite behaves the same way with a 17.5% weight loss in the same temperature range, showing that the amount of PPy in both samples is similar, as expected from the similar synthetic charges and taking into account the experimental uncertainties (electropolymerization yield and charge determination).

Figure 3 displays the CVs of the various materials in the various electrolytic media. It can be noticed that very nice rectangular shapes characteristic of a pure capacitive behavior are obtained in ACN for

all compounds (fig. 3a), while in ACN+IL a small shoulder appears at 0.25 V for nanocomposites (fig. 3b). This can be ascribed to the faradaic component of PPy electrooxidation in this medium. In water, a shrinkage of the electroactive window must be accounted for and the materials cannot be cycled further than 0.4 V without degradation. Based on the measured currents, we can estimate that the gain between starting graphene and final nanocomposites is the highest in ACN and acidic water. In neutral aqueous conditions, a large oxidation current appears for FGS20-bpp/PPy but the lower plateau current tends to demonstrate that PPy is less electroactive in these conditions.

To determine the capacitance values with better accuracy, GCD cycles were recorded with an applied current around 1 A g^{-1}. Figure 4 shows the GCD curves in ACN for all the materials investigated (GCD curves in other media are shown in fig. S2). It can be noticed that the ohmic drop is weak since a very low potential drop is visible at the time the current is reversed. This is a noticeable difference with the behavior of pure PPy[22]. GCD curves are slightly curved as expected for pseudo-capacitive materials.

Capacitance per mass unit is calculated according to the following equation:

$$C = \frac{\mathrm{Q}}{\mathrm{m}\Delta\mathrm{E}} = \frac{\mathrm{I}\Delta\mathrm{t}}{\mathrm{m}\Delta\mathrm{E}}$$

Where I is the galvanostatic current, $\Delta\mathrm{t}$ the duration of the galvanostatic pulse, $\Delta\mathrm{E}$ the potential variation range and m the weight of coated material.

Specific capacitance values extracted from GCD curves are listed in table 1, along with coulombic efficiencies estimated from the ratio of discharge vs. charge times. These latter are all above 83% demonstrating the absence of significant degradation of the materials. It is clear that FGS20 and FGS20-bpp show similar capacitance values in all electrolytic media, while incorporating PPy significantly raises the capacitance of the final material as expected for a pseudo-capacitive additional component. The highest values are obtained in acidic medium for FGS20 and FGS20-bpp and in ACN+IL for nanocomposites including PPy but in this latter case it involves a larger value due

to a faradaic component as can be seen in CVs (fig. 3b). Globally acidic water seems to be the best electrolytic medium to reach the highest capacitance values while keeping a pure capacitive behavior, but ACN offers the advantage of a larger electroactivity window, which leads to higher values for energy stored at the end.

	ACN		Acidic water		Neutral water		ACN+IL	
	SC* ($F\ g^{-1}$)	CE* (%)	SC* ($F\ g^{-1}$)	CE* (%)	SC* ($F\ g^{-1}$)	CE* (%)	SC* ($F\ g^{-1}$)	CE* (%)
FGS20 (1 A g^{-1})	61	92.9	98	97.4	66	97.5	85	86.5
FGS20-bpp (1 A g^{-1})	62	97.5	98	93.2	67	98.2	87	93.1
FGS20/PPy (1.3 A g^{-1})	266	95.7	416	99.2	330	83.8	456	90.5
FGS20-bpp/PPy (1.3 A g^{-1})	285	97.1	417	99.9	340	96.0	485	99.2

*SC= specific capacitance ; CE= coulombic efficency

Table 1 : Capacitance and coulombic efficiency values calculated from galvanic charge-discharge curves

Stability tests have been performed for all materials in the various electrolytes by recording CV after 1500 cycles and comparing them with the first cycle. Figure 5 displays the results in ACN. While pristine FGS remains perfectly stable, FGS20-bpp displays a weak loss which is amplified in the case of composites with PPy. However, the losses remain limited and a stability gain is observed for FGS20-bpp/PPy compared to FGS20/PPy. This is not the case when the potential window is enlarged (see fig. S3). When the potential is cycled up to 1.2 V, a huge loss of capacitance is observed for composites involving PPy and even FGS20-bpp displays a significantly weaker stability than FGS20. For PPy, overoxidation is probably responsible for the performance losses.

Table 2 lists the electroactivity losses recorded for all the materials in the various electrolytic media. The best stability is observed in acetonitrile, and in that solvent functionalized graphene FGS-bpp/PPy nanocomposite appears slightly better that its non-functionalized counterpart FGS/PPy. In

the ACN+IL mixture, the stability is lower than in pure ACN but remains the same for all compounds. This suggests that the underlying graphene stability might be responsible for the overall behavior.

The trend in acidic aqueous solution is more surprising since the stability is enhanced when incorporating PPy. In these conditions, the worst results are obtained for FGS20 with more than 16% loss after 1500 cycles, twice the amount for the other materials. Indeed, FGS20 contains very few polar groups likely to help the compatibility with water and a degradation of the interface upon cycling is observed. Contrarily to what happens in ACN and even in neutral water, composites with PPy are more stable than pristine graphene. The peculiar behavior in acidic water compared with neutral water highlights the role of the cation in the stability. This effect was already noticed by Xu et al. [23] and assigned to the cation size. Indeed, smaller doping ions require less volume changes during the charge storage process and thus the long term stability is enhanced. Furthermore, protons are more mobile than alkali ions and this may also explain why capacitance values are higher in acidic water.

	ACN	Acidic Water	Neutral Water	ACN+IL
FGS20	1.8%	16.6%	15.9%	11.2%
FGS20-bpp	1.5%	9.4%	15.9%	10.3%
FGS20/PPy	8.2%	8.4%	12.4%	11.7%
FGS20-bpp/PPy	5.4%	6.9%	6.9%	11.7%

Table 2: Electroactivity losses extracted from CVs between the first and the 1500th cycle at 100 mVs^{-1}.

Finally, the gradual variation of capacitance measured upon cycling in the various media is represented in figure 6. In ACN (fig. 6a), while FGS20 and FGS20-bpp show fairly constant capacitance upon cycling, the capacitance retention of FGS20/PPy decrease mainly during the first 600 cycles and then stabilize. Adding PPy is globally detrimental for the stability in acetonitrile as demonstrated for PPy alone (see figure 7) but less for the pre-functionalized graphene FGS20-bpp/PPy. Interestingly

the behavior is highly dependent on the electrolytic medium. In the ACN+IL mixture (fig. 6b), all materials behave the same way, with progressive losses down to approximately 10% of the initial capacitance after 1500 cycles. In aqueous acidic medium (fig. 6c), the observed trend is an initial loss for the first 300 cycles followed by a plateau for the further cycles, except for FGS20-bpp/PPy which remains fairly stable along the 1500 cycles. Finally, in neutral water (fig. 6d) the capacitance decrease is very gradual for all materials, with a larger amplitude for composites with PPy. The stability at the end is much better for FGS20-bpp/PPy than for FGS20/PPy, highlighting the beneficial effect of functionalizing graphene prior to electropolymerization.

Comparing these trends to what is observed for pure PPy (fig. 7) in the various investigated media is instructive. In all media, FGS20/PPy and FGS20-bpp/PPy show better stability than PPy alone. The much higher stability of PPy in acidic aqueous electrolyte explains the good performance of FGS20/PPy and FGS20-bpp/Ppy in this medium. While PPy displays a collapse of capacitance in pure acetonitrile, losing 50% of capacity after 1000 cycles, in nanocomposites the performances remain at a very high level (above 90%) underlining the positive role of the graphene underlayer. The same conclusion can be drawn in neutral water where the capacitance decrease upon cycling is similar for pure PPy and FGS/PPy nanocomposites but FGS-bpp/PPy shows a drop limited to 75% (vs. 70%) of the initial value compared to PPy and FGS20/PPy. In that case, this highlights the benefit of surface modification of graphene sheets before adding PPy. It can thus be concluded that functionalizing graphene before incorporating PPy has a positive impact on stability in all media but ACN+IL (but in that electrolyte all materials behave similarly) and that graphene/PPy nanocomposites exhibit much higher stability than PPy alone and in one case (acidic medium) than graphene alone, which was somehow unexpected. This can be understood by considering interfacial properties, since modifying graphene surface also leads to a better stability in acidic solution. Adding basic functions like pyridine may help to incorporate more protons (higher capacitance) and accommodate the surface exchanges upon repeated cycling (more stability). In nanocomposites, the surface tension between PPy and graphene being lower for FGS-bpp, volume changes occurring in PPy upon cycling can involve the

whole material leading to a better stability of FGS-bpp/PPy vs. FGS/PPy, the effect being more sensitive in ACN and neutral water where larger ion sizes must be accounted for.

Conclusion

We have investigated the impact of functionalizing graphene sheets by pyridine substituted pyridazine prior to electropolymerization of pyrrole to design functionalized graphene/polypyrrole nanocomposites. The specific capacitances of the various materials were measured in various electrolytic media. The highest capacitance values are obtained in acidic water while in acetonitrile, a pure capacitive behavior can be seen for all materials including nanocomposites. Stability tests show a positive impact of graphene functionalization prior to pyrrole electropolymerization was found in all media except the ionic liquid/acetonitrile mixture where all materials behave the same way. In acidic water an unexpected trend has been observed where nanocomposites are more stable than pristine graphene itself. In this latter case the nanocomposite made of modified graphene and polypyrrole display a very high stability with less than 5% loss after 1500 cycles. This result is important since long term stability was identified as a weak point of conducting polymers in supercapacitor materials for a long time.

Acknowledgments

Pr I. Aksay and Dr D. Dabbs (Princeton University) are warmly acknowledged for providing FGS20.

Indonesian endowment fund for education (LPDP) is acknowledged for funding the PhD of Yahdi Bin Rus.

References

[1] G.A. Snook, P. Kao, A.S. Best, Conducting-polymer-based supercapacitor devices and electrodes, *Journal of Power Sources*, 196 (2011) 1-12.

[2] B.E. Conway, Electrochemical supercapacitors: scientific fundamentals and technological applications, Springer1999.

[3] Y.S. Lim, Y.P. Tan, H.N. Lim, N.M. Huang, W.T. Tan, Preparation and characterization of polypyrrole/graphene nanocomposite films and their electrochemical performance, *Journal of Polymer Research*, 20 (2013).

[4] H.P. de Oliveira, S.A. Sydlik, T.M. Swager, Supercapacitors from Free-Standing Polypyrrole/Graphene Nanocomposites, *Journal of Physical Chemistry C*, 117 (2013) 10270-10276.

[5] S.K. Kandasamy, K. Kandasamy, Recent Advances in Electrochemical Performances of Graphene Composite (Graphene-Polyaniline/Polypyrrole/Activated Carbon/Carbon Nanotube) Electrode Materials for Supercapacitor: A Review, *Journal of Inorganic and Organometallic Polymers and Materials*, 28 (2018) 559-584.

[6] F. Miomandre, P. Audebert, Basics and new insight in the electrochemistry of conducting polymers, in: L.C.P. Almeida (Ed.) Conducting polymers : synthesis, properties and applications, Nova, New York, 2013, pp. 53-90.

[7] S.H. Cho, K.T. Song, J.Y. Lee, Recent Advances in polypyrrole, in: T. Skotheim, J.R. Reynolds (Eds.) *Handbook of conducting polymer* 3rd ed, CRC Press, Boca Raton, 2007.

[8] H. Lee, H. Kim, M.S. Cho, J. Choi, Y. Lee, Fabrication of polypyrrole (PPy)/carbon nanotube (CNT) composite electrode on ceramic fabric for supercapacitor applications, *Electrochimica Acta*, 56 (2011) 7460-7466.

[9] X. Li, I. Zhitomirsky, Electrodeposition of polypyrrole-carbon nanotube composites for electrochemical supercapacitors, *Journal of Power Sources*, 221 (2013) 49-56.

[10] A. Afzal, F.A. Abuilaiwi, A. Habib, M. Awais, S.B. Waje, M.A. Atieh, Polypyrrole/carbon nanotube supercapacitors: Technological advances and challenges, *Journal of Power Sources*, 352 (2017) 174-186.

[11] J. Li, Y. Xie, Y. Li, Fabrication of graphene oxide/polypyrrole nanowire composite for high perfor mance supercapacitor electrodes, *Journal of Power Sources* 241 (2013) 388-395.

[12] H.-H. Chang, C.-K. Chang, Y.-C. Tsai, C.-S. Liao, Electrochemically synthesized graphene/polypyrrole composites and their use in supercapacitor, *Carbon*, 50 (2012) 2331-2336.

[13] D. Zhang, X. Zhang, Y. Chen, P. Yu, C. Wang, Y. Ma, Enhanced capacitance and rate capability of graphene/polypyrrole composite as electrode material for supercapacitors, *Journal of Power Sources*, 196 (2011) 5990-5996.

[14] W.S. Hummers, R.E. Offeman, Preparation of Graphitic Oxide, *Journal of the American Chemical Society*, 80 (1958) 1339-1339.

[15] T. Ramanathan, A.A. Abdala, S. Stankovich, D.A. Dikin, M. Herrera-Alonso, R.D. Piner, D.H. Adamson, H.C. Schniepp, X. Chen, R.S. Ruoff, S.T. Nguyen, I.A. Aksay, R.K. Prud'homme, L.C. Brinson, Functionalized graphene sheets for polymer nanocomposites, *Nature Nanotechnology*, 3 (2008) 327-331.

[16] M.J. McAllister, J.-L. Li, D.H. Adamson, H.C. Schniepp, A.A. Abdala, J. Liu, M. Herrera-Alonso, D.L. Milius, R. Car, R.K. Prud'homme, I.A. Aksay, Single sheet functionalized graphene by oxidation and thermal expansion of graphite, *Chemistry of Materials*, 19 (2007) 4396-4404.

[17] Y. Li, G. Louarn, P.H. Aubert, V. Alain-Rizzo, L. Galmiche, P. Audebert, F. Miomandre, Polypyrrole-modified graphene sheet nanocomposites as new efficient materials for supercapacitors, *Carbon*, 105 (2016) 510-520.

[18] Y.-M. Cai, Z.-y. Qin, L. Chen, Effect of electrolytes on electrochemical properties of graphene sheet covered with polypyrrole thin layer, *Progress in Natural Science: Materials International*, 21 (2011) 460-466.

[19] A. Bello, F. Barzegar, M. J. Madito, D. Y. Momodu, A. A. Khaleed, T. M. Masikhwa, J. K. Dangbegnon and N. Manyala, Electrochemical performance of polypyrrole derived porous activated carbon-based symmetric supercapacitors in various electrolytes, *RSC Advances*, (2016) 6 68141.

[20] Y. Li, F. Miomandre, G. Clavier, L. Galmiche, V. Alain-Rizzo, P. Audebert, Inverse Electron Demand Diels-Alder Reactivity and Electrochemistry of New Tetrazine Derivatives, *Chemelectrochem*, 4 (2017) 430-435.

[21] P. Audebert, F. Miomandre, Electrochemistry of conducting polymers, in: T. Skotheim, J.R. Reynolds (Eds.) *Handbook of conducting polymer*, 3rd ed, CRC Press, Boca Raton, 2007.

[22] C.J. Raj, M. Rajesh, R. Manikandan, S. Park, J.H. Park, K.H. Yu, B.C. Kim, Electrochemical impedance spectroscopic studies on aging-dependent electrochemical degradation of p-toluene sulfonic acid-doped polypyrrole thin film, *Ionics*, 24 (2018) 2335-2342.

[23] J. Zhu, Y. Xu, J. Wang, J. Lin, X. Sun, S. Mao, The effect of various electrolyte cations onelectrochemical performance of polypyrrole/RGO based supercapacitors, *Phys.Chem.Chem.Phys.* 17 (2015) 28666.

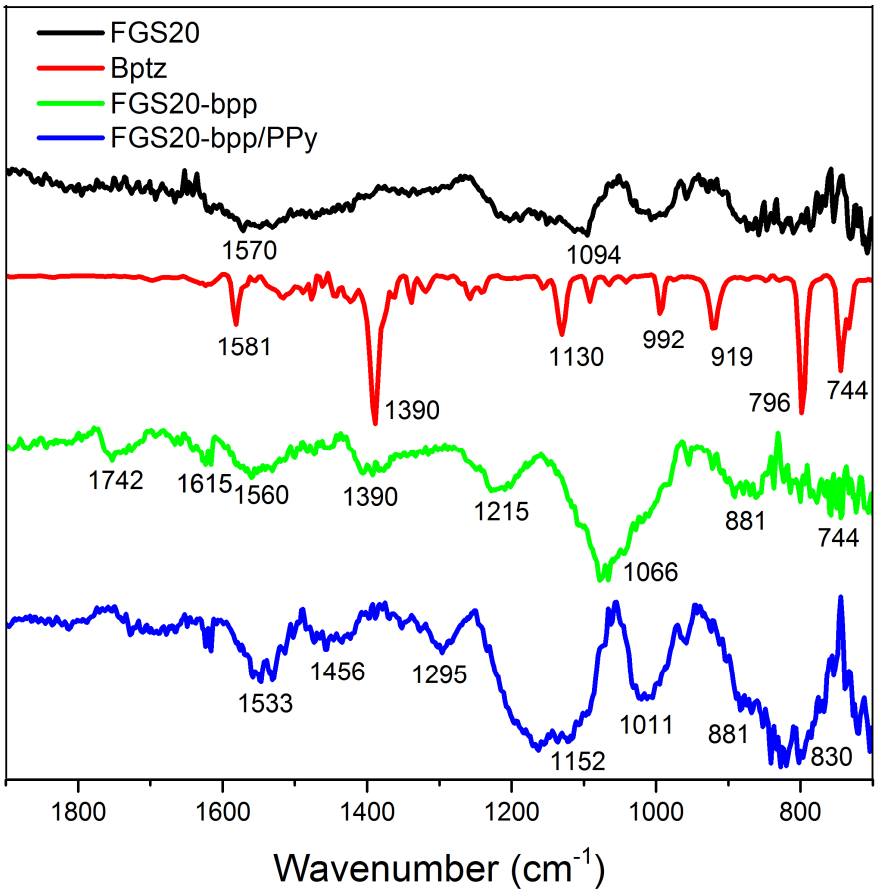

Figure 1: FTIR spectra of FGS20 (black trace), bptz (red trace) and FGS20-bpp (green trace) and FGS20-bpp/PPy (blue trace). All spectra have been normalized for clarity sake.

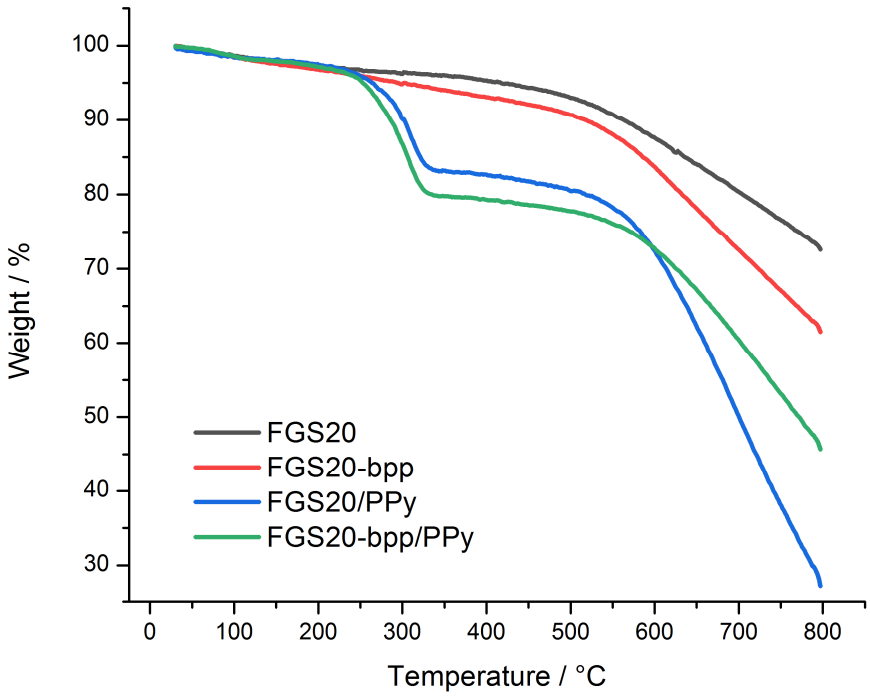

Figure 2 : TGA curves of FGS20 (black), FGS20-bpp (red), FGS20/PPy (blue) and FGS20-bpp/PPy (green) under nitrogen with temperature increase from 30°C to 800°C at 20°C/min.

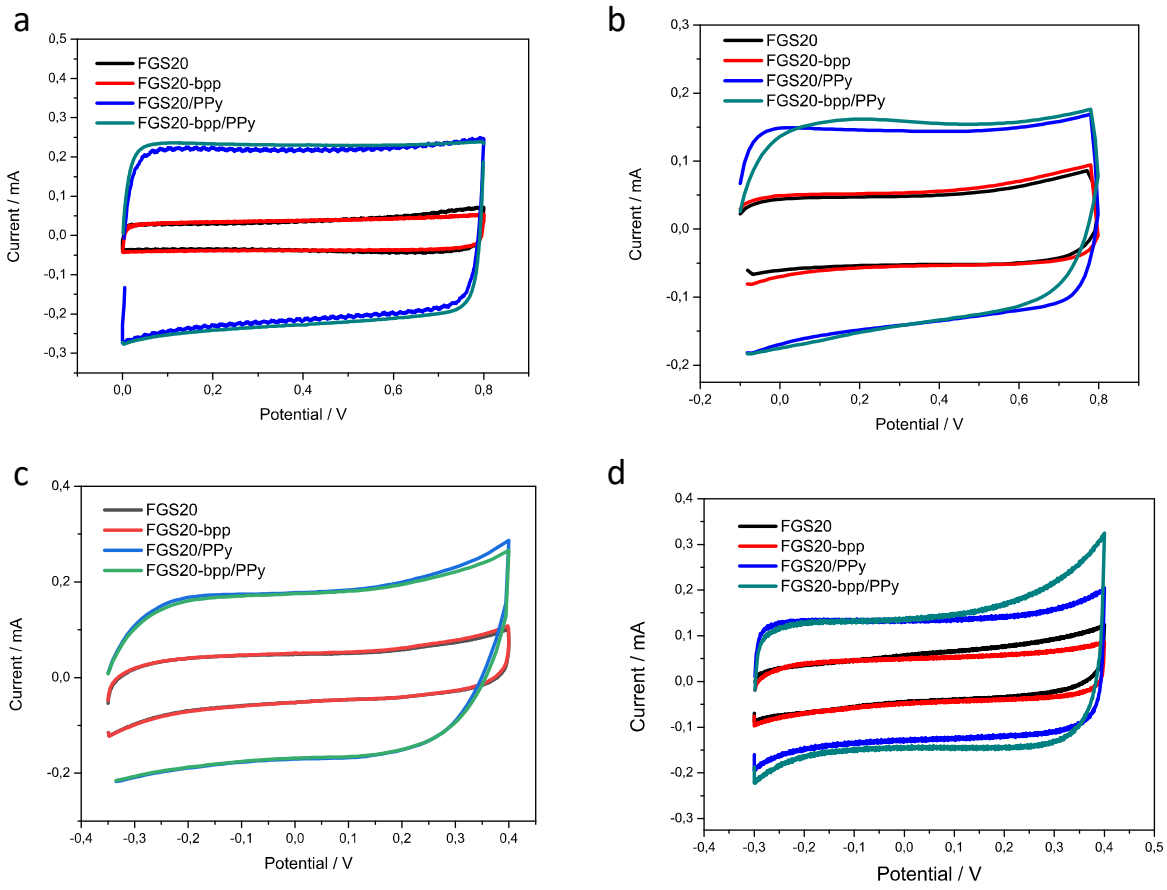

Figure 3: Typical CVs of FGS20 (black), FGS20-bpp (red), FGS20/PPy (blue) and FGS-bpp/PPy (green) at 20 mV/s in acetonitrile (a); acetonitrile + ionic liquid (b); acidic water (c) and neutral water (d).

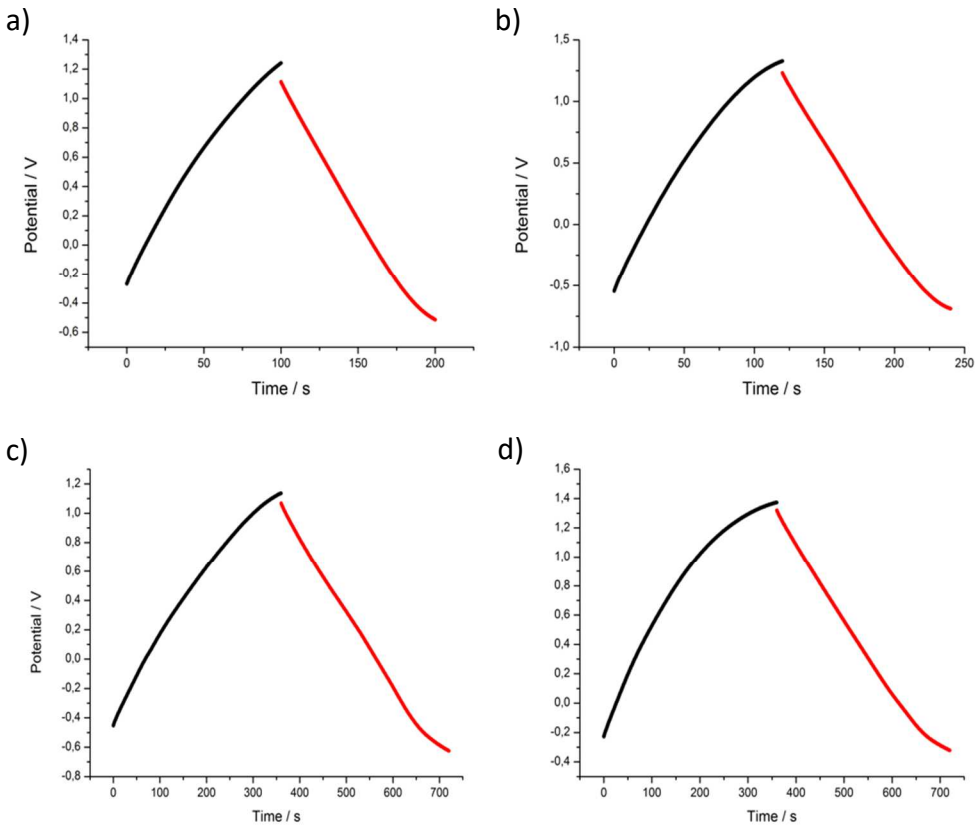

Figure 4 : Galvanostatic charge-discharge tests in acetonitrile for: a) FGS20 (1 A/g); b) FGS20-bpp (1 A/g); c) FGS20/PPy (1.3 A/g) and d) FGS20-bpp/PPy (1.3 A/g).

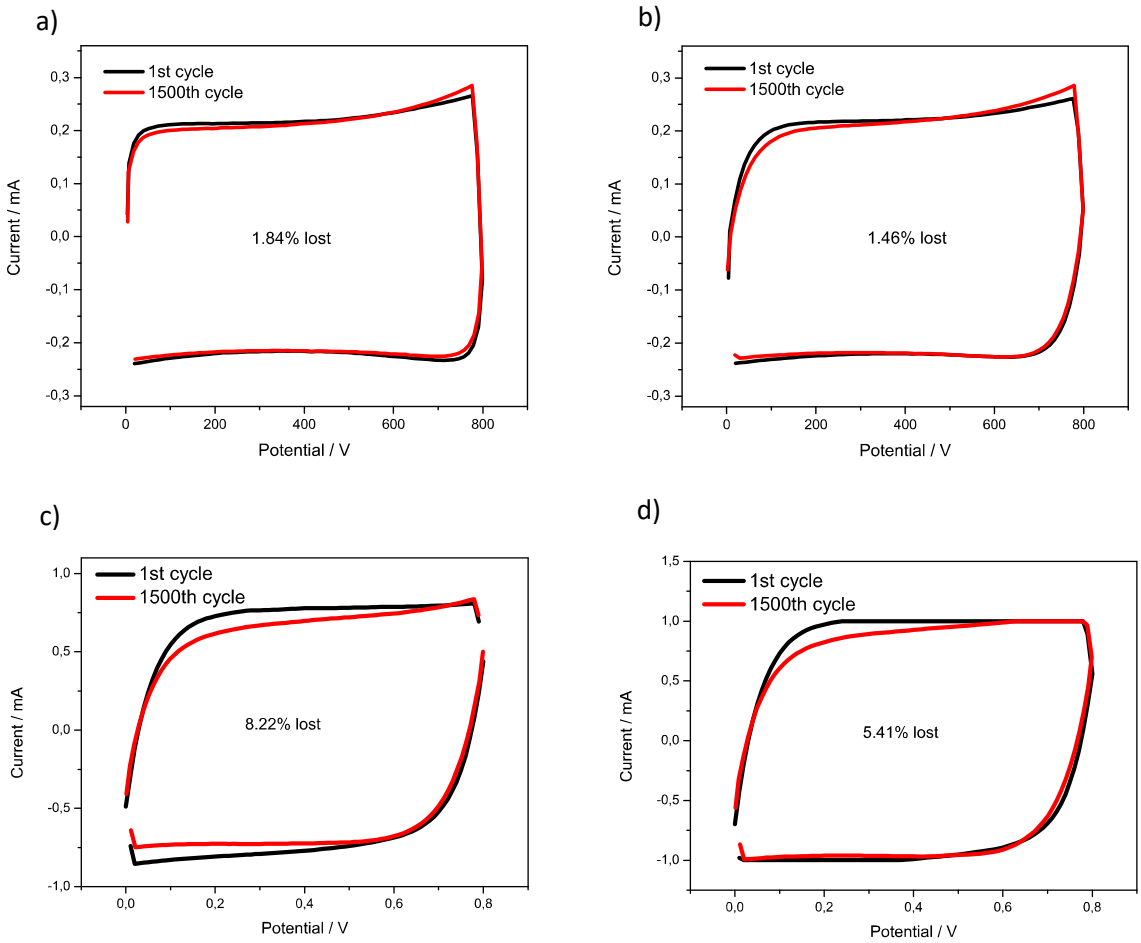

Figure 5: Stability tests by comparison of the 1st and 1500th cycle at 100 mV/s for a) FGS20; b) FGS20-bpp; c) PPy/FGS20 and d) PPy/FGS20-bpp in pure acetonitrile

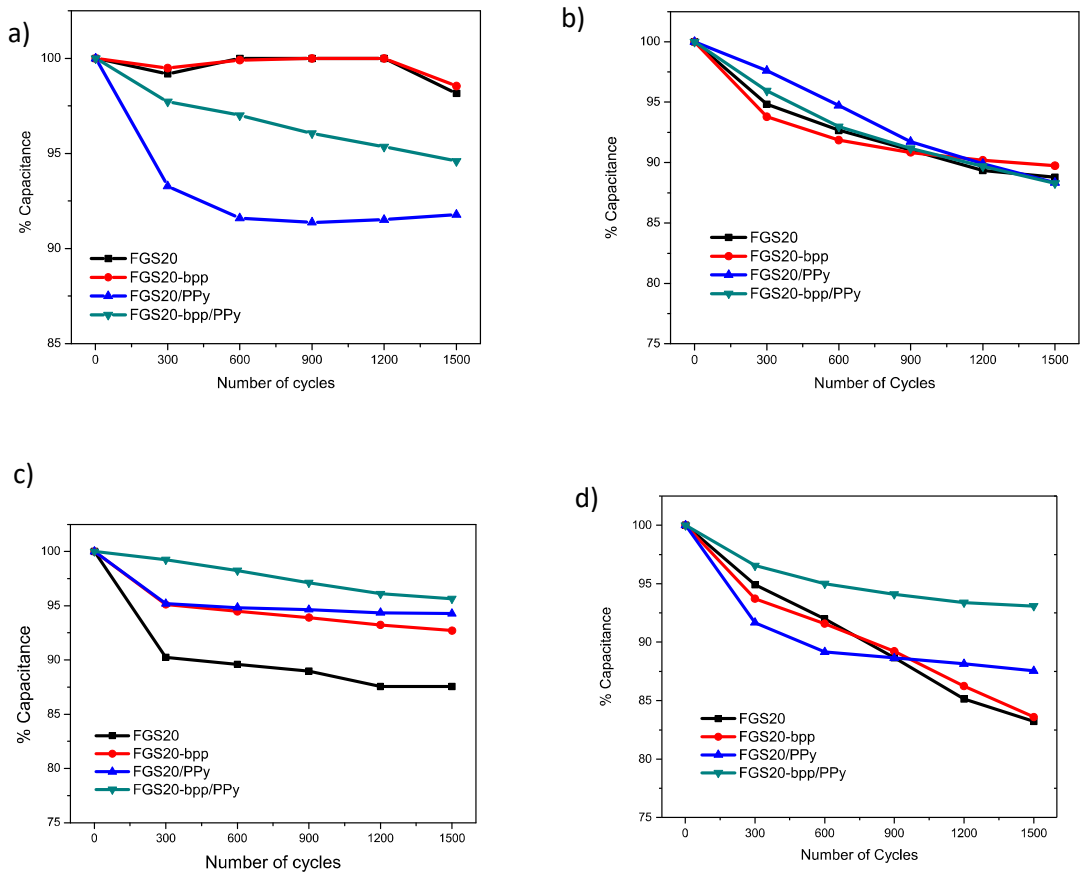

Figure 6: Capacitance retention upon cycling (over the potential range of figure 3) in pure acetonitrile (a); acetonitrile + ionic liquid (b); acidic (0.01 M H_2SO_4) (c) and neutral (0.1 M Na_2SO_4) (d) aqueous solutions. Same color code for materials as in figure 3.

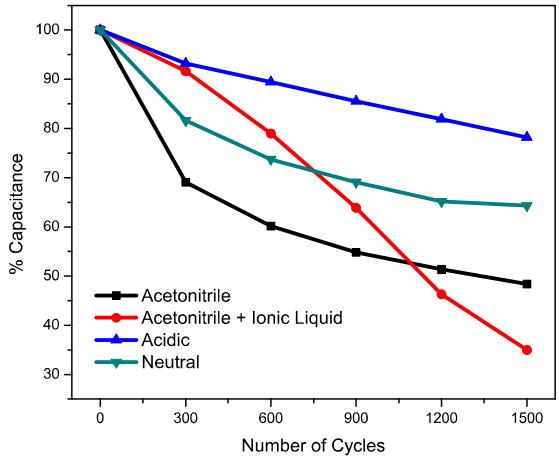

Figure 7: Capacitance retention of PPy upon cycling (over the potential range of figure 3) in pure acetonitrile (black); acetonitrile + ionic liquid (red); acidic (0.01 M H_2SO_4) (blue) and neutral (0.1 M Na_2SO_4) (green) aqueous solutions.